Deriving the hygroscopicity of ambient particles using low-cost optical particle counters

Wei-Chieh Huang[1], Hui-Ming Hung[1*], Ching-Wei Chu[1], Wei-Chun Hwang[1], and Shih-Chun Candice Lung[2]

5 [1]Department of Atmospheric Sciences, National Taiwan University, Taipei, 106319, Taiwan
[2] Research Center for Environmental Changes, Academia Sinica, Taipei, 115201, Taiwan

Correspondence to: Hui-Ming Hung (hmhung@ntu.edu.tw)

Abstract. This study investigates the chemical composition and physical properties of aerosols, which play a crucial role in influencing human health, cloud physics, and local climate. Our focus centers on the hygroscopicity of ambient aerosols, a key

10 property reflecting the ability to absorb moisture from the atmosphere and serve as cloud condensation nuclei. Employing home-built Air Quality Box (AQB) systems equipped with low-cost sensors, we assess the ambient variability of particulate matter (PM) concentrations to determine PM hygroscopicity. The AQB systems effectively captured meteorological parameters and most pollutant concentrations, showing high correlations with data from the Taiwan Environmental Protection Administration (TW-EPA). With the application of κ-Köhler equation and certain assumptions, AQB-monitored PM

15 concentrations are converted to dry particle mass concentration, providing optical particles counter sensitivity correction and resulting in improved correlation with TW-EPA data. The derived κ values range from 0.15 to 0.29 for integrated fine particles ($PM_{2.5}$) and 0.05 to 0.13 for coarse particles ($PM_{2.5-10}$), consistent with results of ionic chromatography analysis from a previous winter campaign nearby. Moreover, the analysis of PM_{10} division into $PM_{2.5}$ and $PM_{2.5-10}$, considering composition heterogeneity, provided improved dry PM_{10} concentration as the sensitivity coefficients for $PM_{2.5-10}$ were notably higher than

20 for $PM_{2.5}$. Our methodology provides a comprehensive approach to assess ambient aerosol hygroscopicity, with significant implications for atmospheric modeling, particularly in evaluating aerosol efficiency as cloud condensation nuclei and in radiative transfer calculations. Overall, the AQB systems proved to be effective in monitoring air quality and deriving key aerosol properties, contributing valuable insights into atmospheric science.

1 Introduction

25 In an era of increased industrialization, individuals face growing exposure to poor air quality, elevating the risks of cardiovascular and respiratory diseases (Chen et al., 2017; Brook et al., 2010; Heus et al., 2010). Within the realm of air pollutants, atmospheric aerosols emerge as critical components, playing a vital role in Earth's climate system. They influence radiative balance, cloud formation, and precipitation patterns, while significantly impacting human health, visibility, and ecosystems (Pöschl et al., 2010; Wu et al., 2010; Brook et al., 2010; Hamanaka and Mutlu, 2018). Their ability to scatter and

30 absorb solar radiation, coupled with their role as cloud condensation nuclei (CCNs), emphasizes their significance in shaping both climate dynamics and air quality (Andreae and Rosenfeld, 2008; Rosenfeld et al., 2014; Lohmann and Feichter, 2005). However, understanding the complex interplay between aerosols and these processes requires the physical and chemical properties of aerosols, including hygroscopicity. The hygroscopic growth of aerosol particles, indicating their ability to absorb moisture from the ambient air, alters their size distribution, mass, optical properties, and CCN activity, thereby impacting

35 climate dynamics and air quality (Petters and Kreidenweis, 2007). While traditional methods such as hygroscopicity tandem differential mobility analyzers (HTDMA) and cloud condensation nuclei counters (Chan and Chan, 2005; Hung et al., 2016; Bian et al., 2014) have provided valuable insights into the hygroscopic properties of various aerosol types. However, their complexity and cost often limit their applicability for extensive, long-term measurements.

Over the past decade, the rise in popularity of low-cost optical particle counters (OPCs) can be attributed to their simplicity,

40 portability, and affordability (Sá et al., 2022; Crilley et al., 2018; Samad et al., 2021). OPCs provide real-time data on particle size distributions and mass concentrations with high temporal resolution for monitoring ambient particles. However, challenges arise in ensuring the accuracy of OPCs, necessitating additional constraints or calibrations for optimal performance. The measurement principle of OPCs relies on the dependence of Mie scattering on particle size, yet this dependence is non-monotonic across all sizes. Additionally, particle composition influences light scattering, leading to varying scattering

45 efficiencies (Kaliszewski et al., 2020; Formenti et al., 2021). Variations in particle density directly affect the mass concentration derived from the monitored number size concentration (Hagan and Kroll, 2020; Dacunto et al., 2015). A particularly challenging issue involves the removal of absorbed liquid water from ambient particles. Several studies have attempted to derive the dry mass concentration of ambient particles using OPC, employing calibration methods linked to the hygroscopic growth factor (HGF) under controlled relative humidity (RH) conditions. Notably, Crilley et al. (2018) improved

50 OPC mass concentration correction by applying derived κ values of 0.38-0.41 and 0.48-0.51 for $PM_{2.5}$ and PM_{10}, respectively, achieving a 33% improvement. Similarly, Antonio et al. (2018) and Jagatha et al. (2021) elevated calibration from a moderate to a high correlation by assuming a constant κ of 0.40. Furthermore, the chemical composition and physical properties of aerosols exhibit high temporal-spatial variation, making the analysis and correction of observational data from a physical perspective crucial. The widespread adoption of low-cost sensors, attributed to their affordability, enables more extensive use

55 as users find them more accessible (Castell et al., 2017). This increased utilization enhances spatial resolution in environmental

monitoring, deepening our understanding of pollution evolution. However, it is essential to emphasize that regular maintenance and calibration are necessary for accurate results (Concas et al., 2021; Sá et al., 2022).

In this study, we evaluate the performance of our home-built monitoring systems through a comprehensive analysis and calibration by co-locating them with the Taiwan Environmental Protection Administration (TW-EPA) station. Our primary focus is on OPCs, for which we employed a physical model to elucidate the hygroscopic characteristics of ambient particles during the determination of dry particle mass concentrations for integrated fine particles ($D_p \leq 2.5$ μm) and coarse particles (2.5 μm $< D_p \leq 10$ μm), respectively. Additionally, we discuss various factors contributing to errors in hygroscopicity estimates, aiming to gain valuable insights into using low-cost sensors for extensive and prolonged monitoring applications.

2 Methodology

2.1 AQB system

Two home-built AQB systems (AQB #1 and AQB #2) consist of multiple sensors that monitor meteorological parameters such as temperature (T), relative humidity (RH), and pressure (P), as well as gaseous species, and particulate matter (PM) with a temporal resolution of seconds as shown in Fig. 1 with sensor information summarized in Table S1. The gas sensors include five Alphasense amperometric B4 series sensors that measure CO, NO, NO_2, Ox (O_3+NO_2), and SO_2, a photo-ionization detector (PID-AH2, Alphasense) monitoring volatile organic compounds, and a non-dispersive infrared CO_2 sensor from Amphenol Advanced Sensors (T6713-5K). The PID sensor, equipped with a Krypton lamp providing a photon energy of about 10.6 eV, cannot detect methane, which has a higher ionization potential of ~13.7 eV (Glockler, 1926). Therefore, the data of non-methane hydrocarbons (NMHC) from TW-EPA is more comparable to PID data in our analysis. The PM sensor (OPC-N2, Alphasense), an optical particle counter, monitors the number size distribution between 0.38 and 17 μm, divided into 16 bins based on Mie scattering, with a sampling flow rate of ~4 mL s^{-1} and a refractive index of 1.5+0 i. In addition, the mass concentration of PM_1, $PM_{2.5}$, and PM_{10} could be calculated from the number size distribution, assuming a particle density of 1.65 g cm^{-3}. These sensors were controlled by a small single-board computer, Raspberry Pi Zero W, at a time resolution of 3 s with data stored in a microSD card and uploaded to cloud storage via 4G LTE. The entire system is housed in a remodeled enclosure measuring 25 cm × 16 cm × 8 cm (L × D × H). The sampling flow rate is controlled by a fan at ~ 5.6 L min^{-1}, corresponding to a residence time of approximately 34 s in the box.

2.2 Calibration campaign and reference data

The calibration of AQB sensors was carried out by co-locating them with TW-EPA Nanzi station in Kaohsiung, Taiwan (22°44'12" N, 120°19'42" E) from 4 to 19 February 2021 (Fig. S1). At Nanzi station, the main gaseous components, dry $PM_{2.5}$ and PM_{10} concentrations, and basic meteorological parameters are continuously monitored with instrumentation information summarized in Table S1. For electrochemical sensors, the performance can be influenced by environmental parameters such

as temperature, relative humidity, and other chemical species that have high cross-sensitivity (Concas et al., 2021; Karagulian et al., 2019; Mead et al., 2013). Therefore, in this study, a linear regression with a multivariate function of voltage and the environmental temperature was applied to retrieve concentrations for gas species. For PM, the reported values from the TW-EPA station (using METONE BAM1020) reflect the dry-state PM concentration by controlling the measurement at RH less than 50% (i.e., a heating device applied to reduce the sampling flow to 35% water saturation when the ambient RH is > 50%). On the contrary, the optical particle counter (OPC) in AQB directly monitors ambient PM concentration. The difference between TW-EPA and AQB reflects the amount of absorbed liquid water in ambient conditions. A simple linear regression between them might not reveal the influence of hygroscopicity completely. Therefore, the κ-Köhler equation (Petters and Kreidenweis, 2007) was applied to derive the κ as discussed in the following section.

2.3 Sensitivity coefficients of OPCs and particle hygroscopicity

To bridge the PM concentration gap between TW-EPA and AQB, the sensitivity correction of OPC and the conversion of ambient particles to dry particles are required. The sensitivity coefficient (α) was evaluated as the ratio of TW-EPA and OPC mass concentration for data at low RH ($\leq 50\%$) having limited water content, as follows:

$$\alpha = \frac{M_{EPA}}{M_{OPC}} \tag{1}$$

where M_{EPA} and M_{OPC} are PM concentrations (μg m^{-3}) measured by TW-EPA and OPC, respectively. RH $\leq$ 50% was applied as the threshold criteria for data selection to determine α, as the mass concentration of ambient particles might have significant water uptake at higher RH. The statistical distribution of M_{EPA} to M_{OPC} ratios at RH $\leq$ 50% was analyzed to assign α as the mean value $\pm 0.5\sigma$ (σ: standard deviation) to prevent high-concentration data points from dominating the statistical result.

The particle size growth with the water saturation ratio (S) for a given hygroscopicity (κ) can be evaluated using κ-Köhler equation as follows (Petters and Kreidenweis, 2007):

$$S = \frac{D_{amb}^3 - D_d^3}{D_{amb}^3 - D_d^3(1-\kappa)} exp(\frac{4\sigma_{s/a}M_w}{RT\rho_w D_{amb}}) \tag{2}$$

where D_{amb} and D_d are the diameters (m) of the ambient and dry particulate matter, respectively, $\sigma_{s/a}$ is the surface tension of the particle (J m^{-2}), M_w is the molecular weight of water (g mole^{-1}), R is the gas constant (J mole^{-1} K^{-1}), and ρ_w is the density of liquid water (1.0 g cm^{-3}). The first term is the solute effect while the second term is the Kelvin effect. As the mass is dominated by the larger particles, the Kelvin effect in Eq. 2 is assumed to be negligible for simplification. The derived dry mass concentration ($M_{d, derived}$) from the measured ambient particles from AQB (M_{OPC}) can be expressed as follows (Pope et al., 2010; Crilley et al., 2018):

$$M_{d,derived} = (\alpha \times M_{OPC}) \times \left[\left(\frac{S\kappa}{1-S}\right) \times \frac{\rho_w}{\rho_d} + 1\right]^{-1} \qquad (3)$$

where ρ_d is the density of dry aerosol particles (assumed to be 1.20 g cm^{-3}). With the determined α values (Eq. 1), κ can be
derived from the data points of aqueous particles at RH above 70%, the deliquescence RH (DRH) verified using IC analyzed
composition with E-AIM model. The mean absolute percentage error (MAPE) parameter between $M_{d,derived}$ and M_{EPA} was used
to assess the appropriate κ value as follow:

$$MAPE = \frac{\sum_{i=1}^{n} \frac{|M_{d,derived,i} - M_{EPA,i}|}{M_{EPA,i}}}{n} \times 100\% \qquad (4)$$

where n is the total number of data points. With the restricted range of α, κ can be derived under the minimum MAPE. Due to
the heterogeneity between particles, PM$_{10}$ was divided into integrated fine particles (D$_p \leq 2.5$ μm) and coarse particles (2.5 μm
< D$_p \leq 10$ μm) to evaluate the individual sensitivity coefficient and hygroscopicity.

2.4 Composition analysis

Hygroscopicity can also be determined using the volume fraction of the major components. Based on an earlier field campaign,
the ion chromatography (IC) method was applied to quantify water soluble components for samples (both PM$_{2.5}$ and PM$_{10}$)
collected at Fooyin University (22°36'09.8" N, 120°23'23.1" E) in Kaohsiung from 15 to 28 January 2013. Ambient aerosol
samples were collected using a pair of dichotomous aerosol samplers (Model: RP-2025, R&P Co., Inc., Albany, New York)
to collect integrated fine and coarse particles on Teflon filters with sampling flow rates of 15.0 and 16.7 L min^{-1}, respectively.
The samples were categorized into daytime and nighttime. Daytime samples were collected from 08:00 to 20:00 local time
(LT), and nighttime samples were collected from 20:00 to 08:00 LT the next day. The samplers were equipped with Teflon
filters deployed for the measurement of water soluble ions (Na$^+$, Mg^{2+}, K$^+$, Ca^{2+}, NH$_4^+$, Cl$^-$, SO$_4^{2-}$, and NO$_3^-$) via ion
chromatography (Model: ICS 1000, Dionex). More information on the chemical analysis method can be found in Salvador and
Chou (2014).

To derive the hygroscopicity from samplings, the ions from IC analysis were converted to chemical components via the
following sequence: ammonium sulfate, ammonium bisulfate, ammonium nitrate (when there is residual ammonium), sodium
nitrate, and sodium chloride. With the assumption of the hygroscopicity of insoluble components as zero and negligible
residual ions contribution (less than 5% of total mass), the overall hygroscopicity can be derived by the volume fraction (ε_i)
weighted hygroscopicity from individual soluble component (i species) as follows:

$$\kappa = \sum_i \varepsilon_i \kappa_i = \sum_i \frac{v_i}{v_{total}} \kappa_i \qquad (5)$$

where κ_i is the hygroscopicity of i species, v_{total} is the volume of particles, and v_i is the volume of i species. The conversion of
particle mass to volume is based on a density of 1.20 g cm^{-3}. The applied hygroscopicity, molecular weight, and density for
the related chemical species are summarized in Table S2. With the assumption that these ions dissolve completely in the

aqueous phase and assuming a van't Hoff factor of 1.0, which represents the maximum estimation, the hygroscopic contributed by the residual ions were found to be approximately up to 1.8% and 6.4% of the overall κ value for $PM_{2.5}$ and $PM_{2.5-10}$, respectively. Given their limited impact on the hygroscopic behavior of the particles, the contribution of the residual ions was

145   not taken into account in the calculation. Additionally, another $PM_{2.5}$ IC data for samples collected at the National Kaohsiung University of Science and Technology (22°46'22.4" N, 120°24'03.4" E) in Kaohsiung for the period of 8 – 18 December 2021smaples was also applied for further comparison (no PM_{10} collection for that campaign). We opted for the 2013 dataset for more discussion due to its comprehensive analysis encompassing both $PM_{2.5}$ and $PM_{2.5-10}$. Furthermore, the composition data obtained from IC analysis was applied to the Extended Aerosol Inorganics Model (E-AIM) Model III (for systems

150   containing H^+, NH_4^+, Na^+, SO_4^{2}, NO_3^-, Cl^-, and H_2O) to evaluate the characteristics of volume variation as a function of RH in the range of 30 to 90% (Clegg et al., 1998). The partitioning of selected trace gases (HNO_3, HCl, NH_3, and H_2SO_4) into the vapor phase was disabled to keep a consistent quantity of applied chemical species in the particle phase. The growth factor, V_{amb}/V_d, above DRH, was applied to retrieve κ value using Eq. 2 but without the Kelvin effect term (Luo et al., 2020). Both the individual sample concentrations and the overall average conditions were analyzed to evaluate the hygroscopic behavior

155   of the particles.

3 Results and Discussion

3.1 Performance of AQB systems

Figure 2 shows the time series of the meteorological parameters and pollutant concentrations between calibrated AQB and TW-EPA data from 14 to 17 February 2021. T, RH, CO, and Ox showed a good correlation with r > 0.9, while NO, NO_2,

160   $PM_{2.5}$, and PM_{10} had a moderate correlation (r ≥ 0.48). The PID sensor had consistent peaks with high NMHC concentrations and could not reveal temporal variation at low concentrations, resulting in a low correlation. Overall, the AQB system performs well in capturing the ambient variability of pollutants stated above. The low correlation of SO_2 was due to the cross-sensitivity of this SO_2 sensor, which was highly sensitive to O_3 and NO_2 (about -120% reported in the Technical Specification of Alphasense). O_3 and NO_2 generally have higher concentrations than SO_2 and cause a significant contribution to the response

165   of the SO_2 sensor. However, if high SO_2 concentration events occur, the SO_2 sensor might reflect the variation of SO_2 concentration. The PM concentration in Fig. 2 was calibrated using a simple linear regression, which roughly reflects the trend of mass concentration but shows more significant deviations at higher RH due to the additional absorbed water, as discussed in Sect. 3.2. Most gas species showed a high correlation (r ≥ 0.95) between different AQB systems except for NMHC (r = 0.675) as summarized in Table S3. Further results and discussions focus on the PM analysis using AQB #1, which has a more

170   consistent sampling rate during the observation period, unless stated otherwise.

3.2 Derived Hygroscopicity

Figures 3(a) and 3(c) show the scatter distribution of the mass concentrations between AQB #1 (with no calibration) and TW-EPA data for $PM_{2.5}$ and PM_{10}, respectively. Overall, the PM mass concentrations measured by AQB system appear to be higher than those reported by TW-EPA. The results reveal an apparent influence of ambient RH, indicating the contribution of water content. The red-shaded area represents a regression line with a slope corresponding to the inverse of the sensitivity coefficients (α) derived from data points at ambient RH ≤ 50% (17 out of 356 points, 5%). The notable deviation of the red shaded area from the 1:1 line towards the right side indicates the requirement of $\alpha > 1$ corrections, contributed by the different measurement principles and calibration techniques, which may result from the assuming particle density and refractive index (RI) (dust, density: 1.65 g cm^{-3}, RI: 1.5 + 0i). The estimated α, as summarized in Table 1, are higher for PM_{10} than for $PM_{2.5}$, i.e., 2.02 ± 0.34 vs 1.26 ± 0.16, which are reasonably conclusive as tested with more data points selected at higher RH thresholds (Fig. S2). The α difference between $PM_{2.5}$ and PM_{10} might be attributed to the complex composition of ambient particles, which differs from the samples used for instrument calibration, as well as possible sensitivity variations in OPC over time. With sensitivity calibration, the performance at ambient RH ≤ 50% exhibits a strong correlation with MAPE at 12.8%, 18.5%, and Root Mean Squared Error (RMSE) at 3.7 μg m^{-3}, 10.3 μg m^{-3} for $PM_{2.5}$ and PM_{10}, respectively, as summarized in Table 2 excluding the two significant outliers (shown as hollow circles in Fig. 3). The results confirm the effectiveness of OPCs in capturing PM concentrations, consistent with previous real-time outdoor field studies (Gillooly et al., 2019; Demanega et al., 2021; Sá et al., 2022; Crilley et al., 2018). Additionally, the OPC sampling flow rate has an impact on measurement performance. AQB #1 maintained a steady rate at 3.6 ± 0.2 LPM, whereas AQB #2 exhibits two distinct time periods with sampling flow rates of 3.6-4.2 LPM for the first period and 3.2-3.6 LPM for the second period. The distinctive sampling flow rates result in a non-linear change in α, suggesting the need to separate the data into two parts to estimate the individual α (see Fig. S3).

With the derived α, the hygroscopicities were retrieved using Eq. (3), resulting in κ ranging from 0.18 to 0.29 for $PM_{2.5}$ and 0.20 to 0.39 for PM_{10} (Table 1) during the studied period. Figures 3(d) and 3(f) show the scatter distribution of the derived dry concentration vs. TW-EPA concentration for $PM_{2.5}$ and PM_{10}, respectively. The results from the two AQB systems exhibit slight differences but are consistent overall. Considering both the sensitivity coefficient and hygroscopicity, the performance of AQB in deriving dry PM concentration is significantly improved with lower MAPE, RMSE, and higher R^2 than the results obtained using only the sensitivity coefficient, as summarized in Table 2. However, due to the heterogeneity of composition among different sizes, PM_{10} can be divided into integrated fine particles ($PM_{2.5}$) and coarse particles ($PM_{2.5-10}$, 2.5 μm < D_p ≤ 10 μm) for further analysis. The estimated α value for $PM_{2.5-10,}$ as summarized in Table 1, is approximately one order of magnitude higher than that for $PM_{2.5}$. The lower κ for $PM_{2.5-10}$ might suggest a significant contribution from dust or other less hygroscopic species, consistent with the IC analyses in Table 3 and discussed further in Sect. 3.3. With the retrieved α and κ for $PM_{2.5}$ and $PM_{2.5-10}$, Fig. 3(e) shows the scatter distribution between the derived dry $PM_{2.5-10}$ from AQB data and TW-EPA data, exhibiting a MAPE of 31.8%, more significant than the 24.8% for $PM_{2.5}$. The higher MAPE might result from the low

particle number concentration in the coarse mode, with only about 0.01 to 0.1 particles per bin cm^{-3} in the size range of 3.0 to 10.0 μm. Detection efficiency may be influenced by notable spatial variations, aligning with the findings of Kaliszewski et al. (2020), which showed a reduced correlation between OPC-N3 measurements and reference instruments for larger particles. The dry PM$_{10}$ derived from AQB through the divided PM$_{2.5}$ and PM$_{2.5-10}$ analysis demonstrates better consistency with the reported TW-EPA data than the direct calibration method. This is evidenced by a lower MAPE in Fig. 3(g) (18.2%) compared to Fig. 3(f) (29.2%) and a significant improvement than the simple linear regression method, which has a higher MAPE at 62.5% (Table 2). This substantiates the importance of considering composition heterogeneity among particle sizes for accurate dry PM derivation.

3.3 Aerosol Composition and E-AIM Model

The major soluble composition and concentrations obtained from the IC analysis are summarized in Table 3, showing mean PM$_{2.5}$ and PM$_{2.5-10}$ concentrations of 67 ± 19 and 36 ± 7 μg m^{-3}, respectively. The determined PM$_{2.5}$ soluble composition constitutes approximately 53% of the mass fraction and is predominantly composed of NH$_4^+$, SO$_4^{2-}$, and NO$_3^-$, which are formed through chemical reactions involving industrial and agricultural emissions. In contrast, ~30% of PM$_{2.5-10}$ is soluble components, including NO$_3^-$, SO$_4^{2-}$, Na$^+$, Cl$^-$, NH$_4^+$, and some alkaline earth metal ions (Ca^{2+} and Mg^{2+}), and a more significant proportion is insoluble components (~70%), likely attributed to dust, metallic elements, and unanalyzed organic-components. The increased sea salt content (Na$^+$ and Cl$^-$) is likely transported by the sea breeze during the daytime, while the increased fractions of Ca^{2+} and Mg^{2+} might correspond to sand or dust particles (Li et al., 2022). The temporal variation of derived κ, based on the IC soluble composition analysis, ranges from 0.14 to 0.26 for PM$_{2.5}$ and 0.06 to 0.21 for PM$_{2.5-10}$, as shown in Fig. S4(a) and summarized in Table 1. A similar analysis for the winter of 2021 yielded a consistent κ range for PM$_{2.5}$, as illustrated in Fig. S5. This consistency across distinct study periods indicates typical ambient PM$_{2.5}$ hygroscopic characteristics in Kaohsiung City during winter, which can be applied for further discussion with the AQB data. For coarse particles, the more significant variability in κ for PM$_{2.5-10}$ compared to PM$_{2.5}$ can be attributed to the significant fluctuations in the soluble composition of coarse particles, primarily driven by substantial quantities of thenardite (Na$_2$SO$_4$) and halite (NaCl) (Tang et al., 2019). Due to the dominance of the northeast monsoon wind during the filter sampling period, the influence of the sea-land breeze was relatively weak to cause apparent diurnal variation in κ. The derived κ value for PM$_{2.5}$ from IC analysis (0.14-0.27) is consistent with that obtained from AQB analysis (~0.22), while the κ value for PM$_{2.5-10}$ from IC analysis (0.06-0.21) is relatively higher than that from AQB analysis (~0.09) (Table 1 and Fig. 4(a)). The κ differences between the IC and AQB analyses could be attributed to the spatial and temporal variations in aerosols, as well as the different campaign years and locations (~20 km apart, as shown in Fig. S1). These differences might also be influenced by technique uncertainties, such as ammonia and nitrate sampling evaporation during filter sampling (Hering and Cass, 1999; Chen et al., 2021), as well as OPC detection uncertainties and the required parameter assumption in the calculation. Overall, the derived κ values from the OPC data in AQB likely reflect the mean hygroscopicity of both integrated fine and coarse particles.

The particle growth might follow the κ-Köhler equation (Eq. 2) when all soluble species are fully dissolved, typically occurring above the DRH. With the averaged soluble composition determined from the IC analysis, HGF as a function of RH calculated using E-AIM is shown in Fig. 5. For $PM_{2.5}$, partial deliquescence initiates at 60% of RH with some residual solid components such as $((NH_4)_2SO_4$ and $2NH_4NO_3.(NH_4)_2SO_4)$. Complete dissolution occurs around an RH ~72%. In the case of $PM_{2.5-10}$, water uptake begins at 42% RH, leaving a residual solid composed of $3NH_4NO_3(NH_4)_2SO_4$, NH_4Cl, and $NaNO_3.Na_2SO_4.H_2O$ until reaching RH of 68%. The daily DRH happens at 71.3 ± 4.9% and 67.1 ± 3.4% for $PM_{2.5}$ and $PM_{2.5-10}$, respectively, as shown in Figs. S4(b) and S4(c). In the AQB data analysis, an RH threshold of ≤ 50% was applied to determine the sensitivity. At this threshold, $PM_{2.5}$ particles have not yet deliquesced, and $PM_{2.5-10}$ shows minimal volume growth, indicating the applicability of the selected RH threshold for sensitivity calculation. On the other hand, a DRH threshold of 70% was applied to ensure sufficient data points for κ calculation but slightly lower than the DRH of $PM_{2.5}$. To assess the potential bias associated with the selected DRH threshold, Fig. S6 shows the HGF of mean soluble composition as a function of RH estimated using E-AIM. With Eq. 2 (without the Kelvin effect term) and the assumption of volume additivity between particle and uptaken water, κ derived using 70% and 75% thresholds show less than a 1% difference for both integrated fine and coarse compositions, but 13% and 6% less than that estimated from the composition of $PM_{2.5}$ and $PM_{2.5-10}$, respectively. The κ deviation due to the applied threshold appears negligible in this study. The performance is similar to that obtained from the AQB data analysis. As the DRH threshold becomes smaller, the derived κ decreases slightly but with a broader uncertainty (Fig. S7). However, the temporal composition variation in the applied AQB data set (~16 days of observation) might lead to a higher variation. Furthermore, the 13% lower κ for E-AIM than the composition estimation is likely due to the RH-dependent ionic activities following the Zdanovskii-Stokes-Robinson relation in E-AIM. The calculation based on Eq. 2, with volume additivity assumptions, might overestimate the liquid water content. Similar findings were reported by Kreidenweis et al. (2008) regarding the percentage difference between κ-Köhler equation-derived and E-AIM-derived water contents increasing with RH. Overall, κ derived from the growth profile might be smaller than the composition estimation (associated with the cloud nuclei activation), likely due to the assumptions of volume additivity and the fixed van't Hoff factor in the κ-Köhler equation.

3.4 Uncertainty Discussion

For simplicity, we derived κ from AQB data without considering the Kelvin effect and under an assumed particle density. The ignorance of the Kelvin effect might result in minor differences for particles larger than 100 nm under sub-saturated conditions (Pope et al., 2010; Topping et al., 2005; Crilley et al., 2018). To confirm the appropriateness, we assessed biases for particles at 0.1 and 1 µm without considering the Kelvin effect, as shown in Fig. S8. For particles with a κ value of 0.3 under RH ranging from 70% to 95%, the deviation of κ due to neglecting the Kelvin effect is -10% for 0.1 µm particles and -1% for 1 µm particles, decreasing with particle diameter. The growing particle diameter is overestimated under the same RH conditions because the positive Kelvin effect is ignored. To compensate for the deficiency in saturation, the balanced particle diameter needs to be more significant with a larger solute effect. However, the average mass-weighted mean diameter for $PM_{2.5}$ is about 1.3 µm. Therefore, the ignorance of Kelvin's effect in our analysis has limited influence on the derived κ. This influence becomes more

significant with increasing RH, resulting in a more considerable underestimation of κ values under high RH conditions. During our monitoring campaign, the surrounding RH ranged from 31 to 92%, and we focused on deriving κ values for integrated fine and coarse particles. Therefore, the assumption of a negligible Kelvin effect is proper for this study.

Furthermore, the derived κ using Eq. (3) for AQB data or Eq. (5) for IC data is notably influenced by the assumed particle density. Assuming that the undetermined composition mainly consists of secondary organic species, having a density of 1.2 g cm^{-3}, within the reported densities ranging from 0.9 to 1.6 g cm^{-3} depending on the formation process (Malloy et al., 2009; Kostenidou et al., 2007; Zelenyuk et al., 2008), along with the properties of analyzed soluble chemical species summarized in Table S2, the calculated densities for $PM_{2.5}$ and $PM_{2.5-10}$ are 1.42 ± 0.03 and 1.34 ± 0.07 g cm^{-3}, respectively (Fig. S9). This increases densities by about 15% and 10% for $PM_{2.5}$ and $PM_{2.5-10}$, respectively. Consequently, the derived κ from AQB data increases by approximately 17% and 9% for $PM_{2.5}$ and $PM_{2.5-10}$, respectively, while the derived κ from IC data is proportional to density (i.e., 15% and 10% for $PM_{2.5}$ and $PM_{2.5-10}$, respectively) as shown in Fig. 4(b). Overall, the derived κ exhibits consistency between the AQB and IC analysis. This bias might be intensified if components having a higher portion of composition with a higher density, such as black carbon (a non-hygroscopic species with κ~0) having a high density of about 1.8 g cm^{-3} (Park et al., 2004; Shiraiwa et al., 2008) are taken into consideration.

4 Conclusion

In this study, we evaluated the performances of home-built Air Quality Box (AQB) systems equipped with low-cost sensors and focused on the ambient variability of particulate matter (PM) concentrations to derive the hygroscopicity of PM and the conversion to dry particle concentrations. The AQB systems revealed their effectiveness in capturing meteorological parameters and most pollutant concentrations with high correlations ($r \geq 0.96$) for temperature, relative humidity, CO, and Ox ($O_3 + NO_2$) and moderate correlations ($r \geq 0.48$) for NOx and PM, as compared to TW-EPA data. In the PM analysis, PM_{10} was divided into $PM_{2.5}$ and $PM_{2.5-10}$ to account for compositional heterogeneity among different particle sizes. Comparing the AQB-monitored ambient PM data and the TW-EPA data (for dry particles) at RH ≤ 50%, the derived sensitivity coefficients (α) for $PM_{2.5-10}$ (10.58 - 12.37) were higher than those for $PM_{2.5}$ (1.26 - 1.44) likely due to the significant sensitivity variation in the OPC over time. By considering hygroscopicity with the κ-Köhler equation and assuming a constant composition density for sensitivity-corrected AQB data, the derived dry particle mass concentrations show improved consistency with TW-EPA data compared to the simple linear regression approach. The derived κ values range from 0.15 to 0.29 for $PM_{2.5}$ and 0.05 to 0.13 for $PM_{2.5-10}$, consistent with those from IC soluble composition analysis (0.14 to 0.27 for $PM_{2.5}$ and 0.06 to 0.21 for $PM_{2.5-10}$) and primarily influenced by the proportion of soluble components, ~53% in $PM_{2.5}$ and ~30% in $PM_{2.5-10}$. The sensitivity analysis of various parameters showed that the effects of chosen deliquescence relative humidity (DRH) thresholds and Kelvin effects had a minor impact on κ values (less than 1%). Conversely, recalculating particle densities for $PM_{2.5}$ (1.42 ± 0.03 g cm^{-3}) and $PM_{2.5-10}$ (1.34 ± 0.07 g cm^{-3}) led to higher κ values by approximately 17% and 9%, respectively, compared to the results assuming 1.2 g cm^{-3}. Overall, the AQB systems are helpful in understanding the temporal and spatial variability of air quality

by effectively monitoring pollutant concentrations and providing the capability for hygroscopicity derivation. This study also emphasizes the need for careful consideration of uncertainties and calibration techniques to accurately interpret low-cost sensor data in atmospheric research.

Code & Data availability

305 The code is not publicly accessible, but readers can contact HM Hung (hmhung@ntu.edu.tw) for more information. The observation data for AQBs and TW-EPA, the E-AIM model output, and the hygroscopicity deriving result used in this study can be accessed online at https://github.com/NTUACLab/Wei-Chieh.

Author contributions

310 WC Huang carried out the calibration campaign, did data analysis, and prepared the manuscript draft. HM Hung supervised the project, including data discussion and manuscript editing. CW Chu and WC Hwang designed the home-built AQB system and did database generation. SCC Lung supervised the field study of 2013 and carried out the aerosol composition analysis in 2021.

Competing interests

315 The authors declare that they have no conflict of interest.

Acknowledgments

We appreciate Taiwan EPA for providing the minute-averaged data of meteorological parameters and chemical species for calibration and comparison and Dr. Shih-Chieh Hsu at Research Center for Environmental Changes, Academia Sinica, Taipei,
320 for composition data of $PM_{2.5}$ and PM_{10} in Kaohsiung (2013). This study was supported by the National Science and Technology Council in Taiwan (111-2111-M-002-009 and 112-2111-M-002-014).

References

Andreae, M. O. and Rosenfeld, D.: Aerosol–cloud–precipitation interactions. Part 1. The nature and sources of cloud-active aerosols, Earth-Sci. Rev., 89, 13-41, https://doi.org/10.1016/j.earscirev.2008.03.001, 2008.

325   Bian, Y. X., Zhao, C. S., Ma, N., Chen, J., and Xu, W. Y.: A study of aerosol liquid water content based on hygroscopicity measurements at high relative humidity in the North China Plain, Atmos. Chem. Phys., 14, 6417-6426, 10.5194/acp-14-6417-2014, 2014.

Brook, R. D., Rajagopalan, S., Pope, C. A., Brook, J. R., Bhatnagar, A., Diez-Roux, A. V., Holguin, F., Hong, Y., Luepker, R. V., Mittleman, M. A., Peters, A., Siscovick, D., Smith, S. C., Whitsel, L., and Kaufman, J. D.: Particulate Matter Air
330   Pollution and Cardiovascular Disease, Circulation, 121, 2331-2378, 10.1161/CIR.0b013e3181dbece1, 2010.

Castell, N., Dauge, F. R., Schneider, P., Vogt, M., Lerner, U., Fishbain, B., Broday, D., and Bartonova, A.: Can commercial low-cost sensor platforms contribute to air quality monitoring and exposure estimates?, Environ. Int., 99, 293-302, 10.1016/j.envint.2016.12.007, 2017.

Chan, M. N. and Chan, C. K.: Mass transfer effects in hygroscopic measurements of aerosol particles, Atmos. Chem. Phys., 5,
335   2703-2712, 10.5194/acp-5-2703-2005, 2005.

Chen, C. L., Chen, T. Y., Hung, H. M., Tsai, P. W., Chou, C. C. K., and Chen, W. N.: The influence of upslope fog on hygroscopicity and chemical composition of aerosols at a forest site in Taiwan, Atmos. Environ., 246, 10.1016/j.atmosenv.2020.118150, 2021.

Chen, S. Y., Chan, C. C., and Su, T. C.: Particulate and gaseous pollutants on inflammation, thrombosis, and autonomic
340   imbalance in subjects at risk for cardiovascular disease, Environ. Pollut., 223, 403-408, 10.1016/j.envpol.2017.01.037, 2017.

Clegg, S. L., Brimblecombe, P., and Wexler, A. S.: Thermodynamic model of the system H^+-NH_4^+-Na^+-SO_4^{2-}-NO_3^--Cl^--H_2O at 298.15 K, J. Phys. Chem. A, 102, 2155-2171, 10.1021/jp973043j, 1998.

Concas, F., Mineraud, J., Lagerspetz, E., Varjonen, S., Liu, X. L., Puolamaki, K., Nurmi, P., and Tarkoma, S.: Low-Cost Outdoor Air Quality Monitoring and Sensor Calibration: A Survey and Critical Analysis, ACM Trans. Sens. Netw., 17,
345   10.1145/3446005, 2021.

Crilley, L. R., Shaw, M., Pound, R., Kramer, L. J., Price, R., Young, S., Lewis, A. C., and Pope, F. D.: Evaluation of a low-cost optical particle counter (Alphasense OPC-N2) for ambient air monitoring, Atmos. Meas. Tech., 11, 709-720, 10.5194/amt-11-709-2018, 2018.

Dacunto, P. J., Klepeis, N. E., Cheng, K.-C., Acevedo-Bolton, V., Jiang, R.-T., Repace, J. L., Ott, W. R., and Hildemann, L.
350   M.: Determining $PM_{2.5}$ calibration curves for a low-cost particle monitor: common indoor residential aerosols, Environ. Sci.: Process. Impacts, 17, 1959-1966, 10.1039/c5em00365b, 2015.

Demanega, I., Mujan, I., Singer, B. C., Andelkovic, A. S., Babich, F., and Licina, D.: Performance assessment of low-cost environmental monitors and single sensors under variable indoor air quality and thermal conditions, Build. Environ., 187, 10.1016/j.buildenv.2020.107415, 2021.

355   Di Antonio, A., Popoola, O. A. M., Ouyang, B., Saffell, J., and Jones, R. L.: Developing a Relative Humidity Correction for Low-Cost Sensors Measuring Ambient Particulate Matter, Sensors, 18, 2790, 2018.

Formenti, P., Di Biagio, C., Huang, Y., Kok, J., Mallet, M. D., Boulanger, D., and Cazaunau, M.: Look−up tables resolved by complex refractive index to correct particle sizes measured by common research−grade optical particle counters, Atmos. Meas. Tech. Discuss., 2021, 1-30, 10.5194/amt-2021-403, 2021.

360   Gillooly, S. E., Zhou, Y., Vallarino, J., Chu, M. T., Michanowicz, D. R., Levy, J. I., and Adamkiewicz, G.: Development of an in-home, real-time air pollutant sensor platform and implications for community use, Environ. Pollut., 244, 440-450, https://doi.org/10.1016/j.envpol.2018.10.064, 2019.

Glockler, G.: The ionization potential of methane, Journal of the American Chemical Society, 48, 2021-2026, 10.1021/ja01419a002, 1926.

365   Hagan, D. H. and Kroll, J. H.: Assessing the accuracy of low-cost optical particle sensors using a physics-based approach, Atmospheric Measurement Techniques, 13, 6343-6355, 10.5194/amt-13-6343-2020, 2020.

Hamanaka, R. B. and Mutlu, G. M.: Particulate Matter Air Pollution: Effects on the Cardiovascular System, Front. Endocrinol., 9, 10.3389/fendo.2018.00680, 2018.

Hering, S. and Cass, G.: The Magnitude of Bias in the Measurement of PM_{25} Arising from Volatilization of Particulate Nitrate
370   from Teflon Filters, J. Air Waste Manag. Assoc., 49, 725-733, 10.1080/10473289.1999.10463843, 1999.

Heus, T., van Heerwaarden, C. C., Jonker, H. J. J., Siebesma, A. P., Axelsen, S., van den Dries, K., Geoffroy, O., Moene, A. F., Pino, D., de Roode, S. R., and de Arellano, J. V. G.: Formulation of the Dutch Atmospheric Large-Eddy Simulation (DALES) and overview of its applications, Geosci. Model Dev., 3, 415-444, 10.5194/gmd-3-415-2010, 2010.

Hung, H.-M., Hsu, C.-H., Lin, W.-T., and Chen, Y.-Q.: A case study of single hygroscopicity parameter and its link to the functional groups and phase transition for urban aerosols in Taipei City, Atmos. Environ., 132, 240-248, https://doi.org/10.1016/j.atmosenv.2016.03.008, 2016.

Kaliszewski, M., Włodarski, M., Młyńczak, J., and Kopczyński, K.: Comparison of Low-Cost Particulate Matter Sensors for Indoor Air Monitoring during COVID-19 Lockdown, Sensors (Basel), 20, 10.3390/s20247290, 2020.

Karagulian, F., Barbiere, M., Kotsev, A., Spinelle, L., Gerboles, M., Lagler, F., Redon, N., Crunaire, S., and Borowiak, A.: Review of the Performance of Low-Cost Sensors for Air Quality Monitoring, Atmos., 10, 10.3390/atmos10090506, 2019.

Kostenidou, E., Pathak, R. K., and Pandis, S. N.: An algorithm for the calculation of secondary organic aerosol density combining AMS and SMPS data, Aerosol Sci. Technol., 41, 1002-1010, 10.1080/02786820701666270, 2007.

Kreidenweis, S. M., Petters, M. D., and DeMott, P. J.: Single-parameter estimates of aerosol water content, Environ. Res. Lett., 3, 035002, 10.1088/1748-9326/3/3/035002, 2008.

Li, J., Liu, W. Y., Castarede, D., Gu, W. J., Li, L. J., Ohigashi, T., Zhang, G. Q., Tang, M. J., Thomson, E. S., Hallquist, M., Wang, S., and Kong, X. R.: Hygroscopicity and Ice Nucleation Properties of Dust/Salt Mixtures Originating from the Source of East Asian Dust Storms, Front. Environ. Sci., 10, 10.3389/fenvs.2022.897127, 2022.

Lohmann, U. and Feichter, J.: Global indirect aerosol effects: a review, Atmos. Chem. Phys., 5, 715-737, 10.5194/acp-5-715-2005, 2005.

Luo, Q., Hong, J., Xu, H., Han, S., Tan, H., Wang, Q., Tao, J., Ma, N., Cheng, Y., and Su, H.: Hygroscopicity of amino acids and their effect on the water uptake of ammonium sulfate in the mixed aerosol particles, Sci. Total Environ., 734, 139318, https://doi.org/10.1016/j.scitotenv.2020.139318, 2020.

Malloy, Q. G. J., Nakao, S., Qi, L., Austin, R., Stothers, C., Hagino, H., and Cocker, D. R.: Real-Time Aerosol Density Determination Utilizing a Modified Scanning Mobility Particle Sizer—Aerosol Particle Mass Analyzer System, Aerosol Sci. Technol., 43, 673-678, 10.1080/02786820902832960, 2009.

Mead, M. I., Popoola, O. A. M., Stewart, G. B., Landshoff, P., Calleja, M., Hayes, M., Baldovi, J. J., McLeod, M. W., Hodgson, T. F., Dicks, J., Lewis, A., Cohen, J., Baron, R., Saffell, J. R., and Jones, R. L.: The use of electrochemical sensors for monitoring urban air quality in low-cost, high-density networks, Atmos. Environ., 70, 186-203, 10.1016/j.atmosenv.2012.11.060, 2013.

Pöschl, U., Martin, S. T., Sinha, B., Chen, Q., Gunthe, S. S., Huffman, J. A., Borrmann, S., Farmer, D. K., Garland, R. M., Helas, G., Jimenez, J. L., King, S. M., Manzi, A., Mikhailov, E., Pauliquevis, T., Petters, M. D., Prenni, A. J., Roldin, P., Rose, D., Schneider, J., Su, H., Zorn, S. R., Artaxo, P., and Andreae, M. O.: Rainforest aerosols as biogenic nuclei of clouds and precipitation in the Amazon, N Y Sci J, 329, 1513-1516, 10.1126/science.1191056, 2010.

Park, K., Kittelson, D. B., Zachariah, M. R., and McMurry, P. H.: Measurement of Inherent Material Density of Nanoparticle Agglomerates, J. Nanoparticle Res., 6, 267-272, 10.1023/B:NANO.0000034657.71309.e6, 2004.

Petters, M. D. and Kreidenweis, S. M.: A single parameter representation of hygroscopic growth and cloud condensation nucleus activity, Atmos. Chem. Phys., 7, 1961-1971, 10.5194/acp-7-1961-2007, 2007.

Pope, F. D., Dennis-Smither, B. J., Griffiths, P. T., Clegg, S. L., and Cox, R. A.: Studies of Single Aerosol Particles Containing Malonic Acid, Glutaric Acid, and Their Mixtures with Sodium Chloride. I. Hygroscopic Growth, J. Phys. Chem. A, 114, 5335-5341, 10.1021/jp100059k, 2010.

Rosenfeld, D., Andreae, M. O., Asmi, A., Chin, M., de Leeuw, G., Donovan, D. P., Kahn, R., Kinne, S., Kivekas, N., Kulmala, M., Lau, W., Schmidt, K. S., Suni, T., Wagner, T., Wild, M., and Quaas, J.: Global observations of aerosol-cloud-precipitation-climate interactions, Rev. Geophys., 52, 750-808, 10.1002/2013rg000441, 2014.

Salvador, C. M. and Chou, C. C. K.: Analysis of semi-volatile materials (SVM) in fine particulate matter, Atmos. Environ., 95, 288-295, https://doi.org/10.1016/j.atmosenv.2014.06.046, 2014.

Samad, A., Mimiaga, F. E. M., Laquai, B., and Vogt, U.: Investigating a Low-Cost Dryer Designed for Low-Cost PM Sensors Measuring Ambient Air Quality, Sensors, 21, 10.3390/s21030804, 2021.

Shiraiwa, M., Kondo, Y., Moteki, N., Takegawa, N., Sahu, L. K., Takami, A., Hatakeyama, S., Yonemura, S., and Blake, D. R.: Radiative impact of mixing state of black carbon aerosol in Asian outflow, J. Geophys. Res. D: Atmos., 113, https://doi.org/10.1029/2008JD010546, 2008.

Sá, J. P., Alvim-Ferraz, M. C. M., Martins, F. G., and Sousa, S. I. V.: Application of the low-cost sensing technology for indoor air quality monitoring: A review, Environ. Technol. Innov., 28, 102551, https://doi.org/10.1016/j.eti.2022.102551, 2022.

Tang, M. J., Zhang, H. H., Gu, W. J., Gao, J., Jian, X., Shi, G. L., Zhu, B. Q., Xie, L. H., Guo, L. Y., Gao, X. Y., Wang, Z., Zhang, G. H., and Wang, X. M.: Hygroscopic Properties of Saline Mineral Dust From Different Regions in China: Geographical Variations, Compositional Dependence, and Atmospheric Implications, J. Geophys. Res. D: Atmos., 124, 10844-10857, 10.1029/2019jd031128, 2019.

Topping, D. O., McFiggans, G. B., and Coe, H.: A curved multi-component aerosol hygroscopicity model framework: Part 1 – Inorganic compounds, Atmos. Chem. Phys., 5, 1205-1222, 10.5194/acp-5-1205-2005, 2005.

Venkatraman Jagatha, J., Klausnitzer, A., Chacón-Mateos, M., Laquai, B., Nieuwkoop, E., van der Mark, P., Vogt, U., and Schneider, C.: Calibration Method for Particulate Matter Low-Cost Sensors Used in Ambient Air Quality Monitoring and Research, Sensors, 21, 3960, 2021.

Wu, C. F., Kuo, I. C., Su, T. C., Li, Y. R., Lin, L. Y., Chan, C. C., and Hsu, S. C.: Effects of Personal Exposure to Particulate Matter and Ozone on Arterial Stiffness and Heart Rate Variability in Healthy Adults, Am. J. Epidemiol., 171, 1299-1309, 10.1093/aje/kwq060, 2010.

Zelenyuk, A., Yang, J., Song, C., Zaveri, R. A., and Imre, D.: A new real-time method for determining particles' sphericity and density: application to secondary organic aerosol formed by ozonolysis of alpha-pinene, Environ. Sci. Technol., 42, 8033-8038, 10.1021/es8013562, 2008.

440 **Tables**

Table 1: The sensitivity coefficients and the hygroscopicity for PM$_{2.5}$, PM$_{10}$, and PM$_{2.5-10}$.

	Sensitivity coefficient (α)		Hygroscopicity (κ)			
	AQB #1	AQB #2*	AQB #1	AQB #2	IC (species)	IC (E-AIM)
PM$_{2.5}$	1.26 ± 0.16	1.44 ± 0.20	0.18 – 0.29	0.15– 0.24	0.14 – 0.27	0.14 – 0.26
PM$_{10}$	2.02 ± 0.34	2.20 ± 0.38	0.20 – 0.39	0.18 – 0.30		
PM$_{2.5-10}$	12.37 ± 1.33	10.58 ± 2.90	0.07 – 0.13	0.05 – 0.09	0.06 – 0.21	0.08 – 0.21

* the sensitivity of AQB #2 presents the value in the period of sampling flow rates at 3.6-4.2 LPM

Table 2: Performance metrics of different calibration methods for $PM_{2.5}$, $PM_{2.5-10}$, and PM_{10}.

	$PM_{2.5}$			$PM_{2.5-10}$			PM_{10}			
	RH≤50% only[a]	All data (no κ)	All data (κ = 0.29)	RH≤50% only[a]	All data (no κ)	All data (κ = 0.09)	RH≤50% only[a]	All data (no κ)	All data (κ = 0.36)	($PM_{2.5}$+ $PM_{2.5-10}$)[c]
applied α	1.26 ± 0.16	1.04	1.40	12.37 ± 1.33	10.77	13.16	2.02 ± 0.34	1.69	2.36	—
MAPE (%)	21.3 (12.8)	48.8	24.8	15.9 (11.5)	37.9	31.8	32.8 (18.5)	62.5	29.2	18.2
RMSE ($\mu g\ cm^{-3}$)	20.5 (3.7)	29.1	11.3	4.9 (2.8)	9.4	9.1	42.6 (10.3)	54.7	26.9	15.9
R^2 [b]	-0.55 (0.51)	-3.49	0.32	0.31 (0.78)	0.57	0.59	-4.18 (-0.58)	-4.74	-0.38	0.51

445 **[a] Only for data points at RH ≤50%. The value in parentheses is the performance result without two significant outliers shown in Fig. 3**

[b] Coefficient of determination (R^2) is calculated as the proportion of variation in the calibrated dry mass concentration.

[c] The combination of calibrated data from $PM_{2.5}$ All data (κ= 0.29) and $PM_{2.5-10}$ All data (κ= 0.09).

Table 3. The total mass concentration, the major water soluble composition and concentration (mean value and standard deviation in µg m^{-3}) of winter PM$_{2.5}$ and PM$_{2.5-10}$ in Kaohsiung by ion chromatography. (others presented the insoluble composition)

Ion species	Total	Na$^+$	Mg^{2+}	K$^+$	Ca^{2+}	NH$_4^+$	Cl$^-$	SO$_4^{2-}$	NO$_3^-$	others
PM$_{2.5}$	67.0 ± 19.2	0.31 ± 0.14	0.06 ± 0.02	0.45 ± 0.14	0.08 ± 0.04	8.24 ± 2.68	1.21 ± 0.91	13.63 ± 4.72	11.89 ± 4.88	31.1 ± 8.0
PM$_{2.5-10}$	36.8 ± 7.64	1.50 ± 0.52	0.21 ± 0.06	0.04 ± 0.02	0.74 ± 0.25	1.07 ± 0.69	1.28 ± 0.69	1.87 ± 1.12	4.35 ± 1.41	25.7 ± 6.4

Figures

455   **Figure 1: The design of the AQB system.**
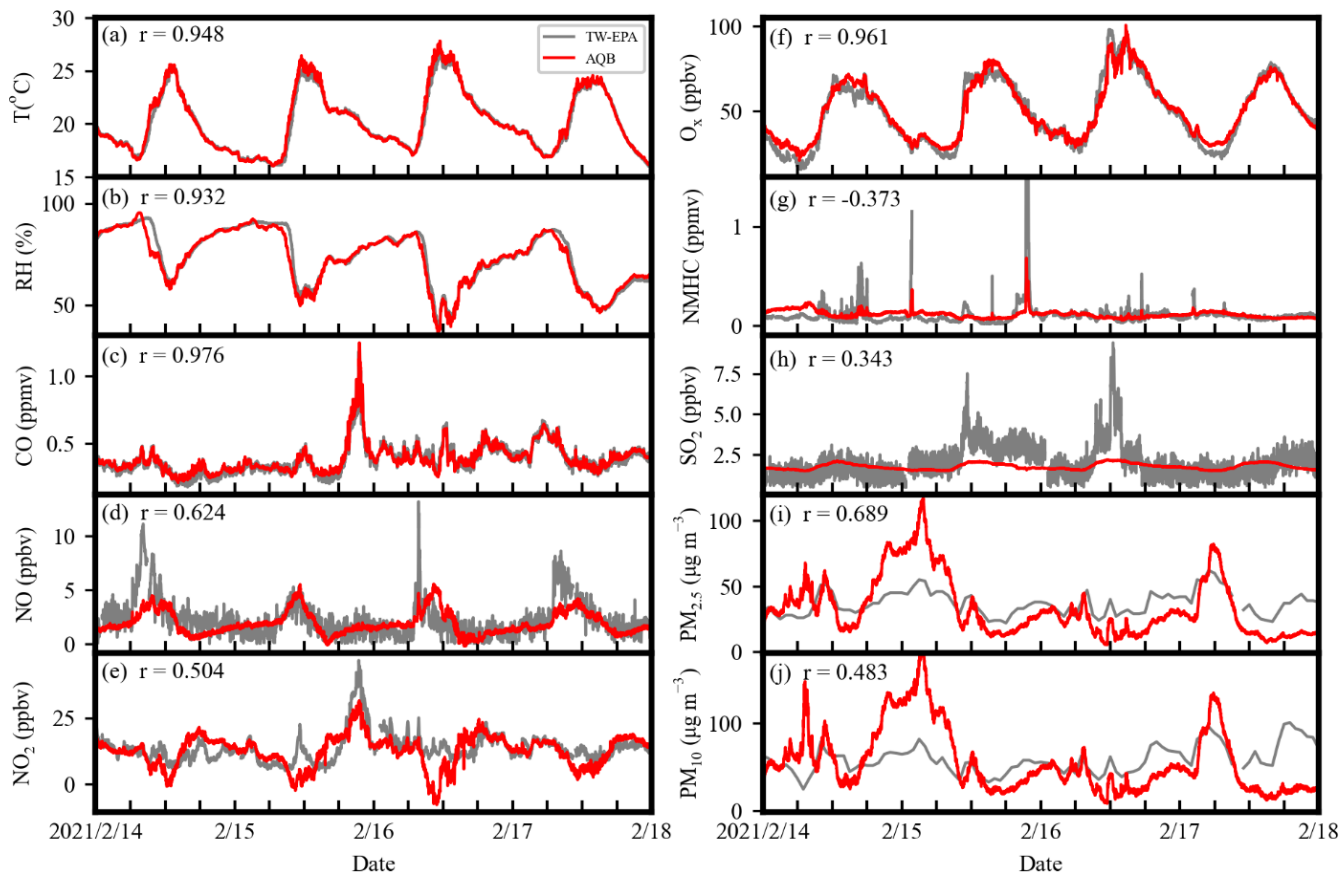
Figure 2: The temporal profiles of calibrated AQB data (red lines) and the TW-EPA measurement (grey lines) for (a) temperature, (b) relative humidity, (c) CO, (d) NO, (e) NO₂, (f) Ox (≡ NO₂ + O₃), (g) Non-methane hydrocarbon, (h) SO₂, (i) PM₂.₅, and (j) PM₁₀ during the period of 14 – 17 February 2021 (4 of 16 days in period). All the species were calibrated using linear regression.

460
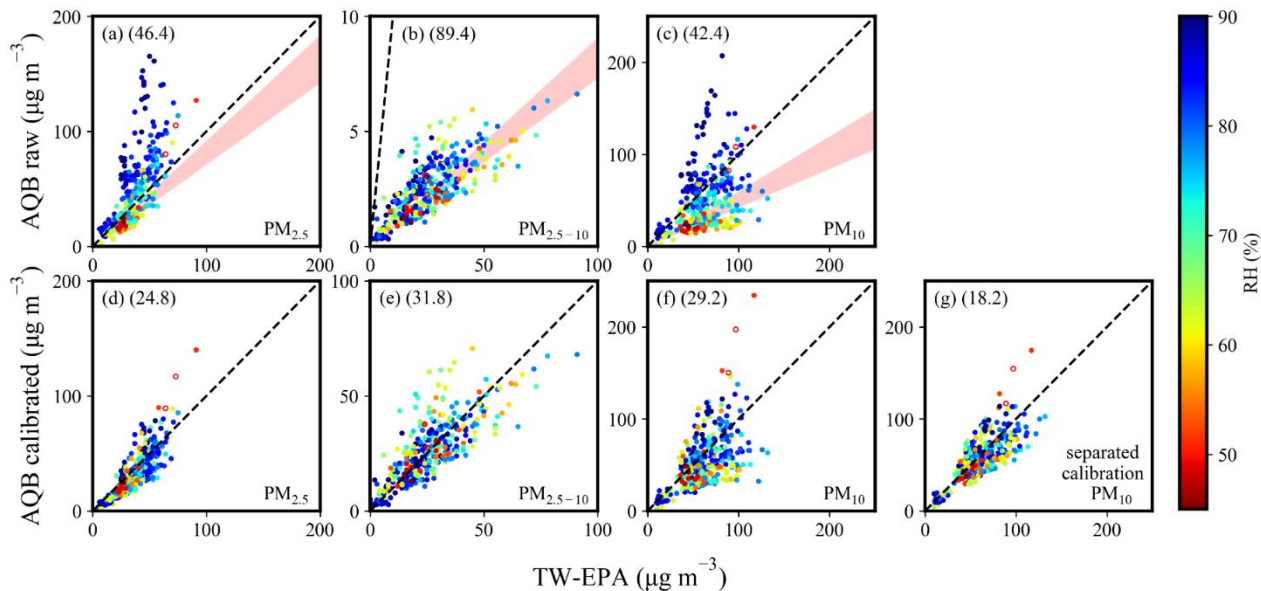
Figure 3: The correlation of mass concentration between TW-EPA and OPC in AQB #1 (raw data or calibrated data): (a, d) PM₂.₅, (b, e) PM₂.₅₋₁₀, (c, f) PM₁₀, and (f) separated calibration PM₁₀, respectively. (a-c) are the raw data, while (d-g) are the calibrated data. The marker color corresponds to relative humidity. The hollow points are the two significant outliers under conditions of RH ≤ 50%. The shaded region represents the data associated with the sensitivity coefficient ("α"). The value in parentheses is the MAPE in percentage.
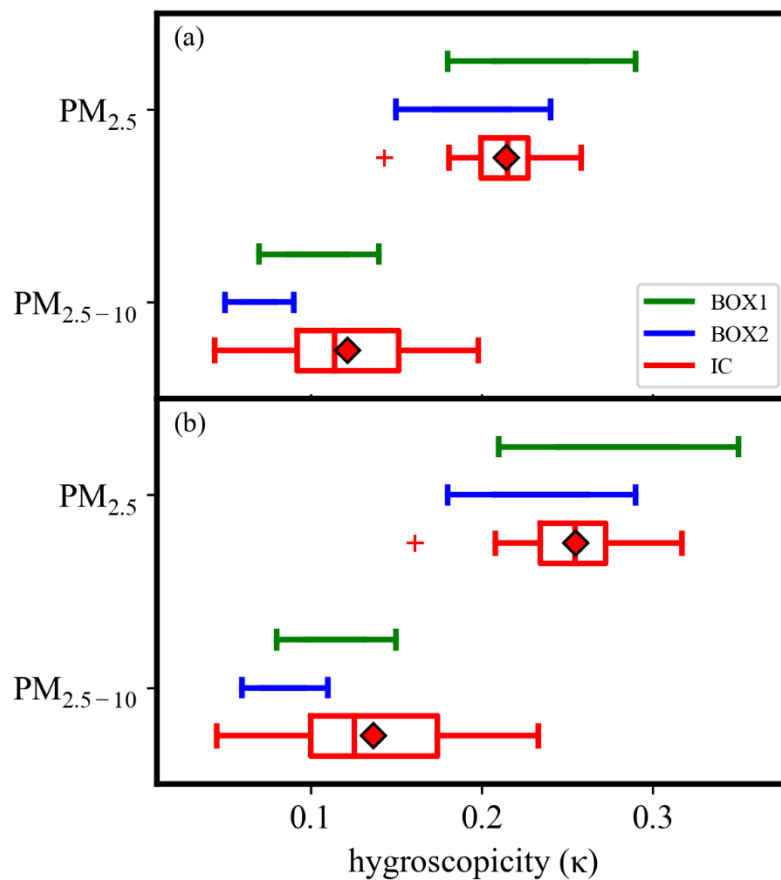
Figure 4: The hygroscopicities of PM$_{2.5}$ and PM$_{2.5-10}$ derived based on data from AQBs and ion chromatography with the assumption particle density of (a) 1.2 g cm^{-3} and (b) 1.42 ± 0.03 and 1.34 ± 0.07 g cm^{-3} for PM$_{2.5}$ and PM$_{2.5-10}$, respectively, based on analyzed composition. The average value is shown as a red diamond.
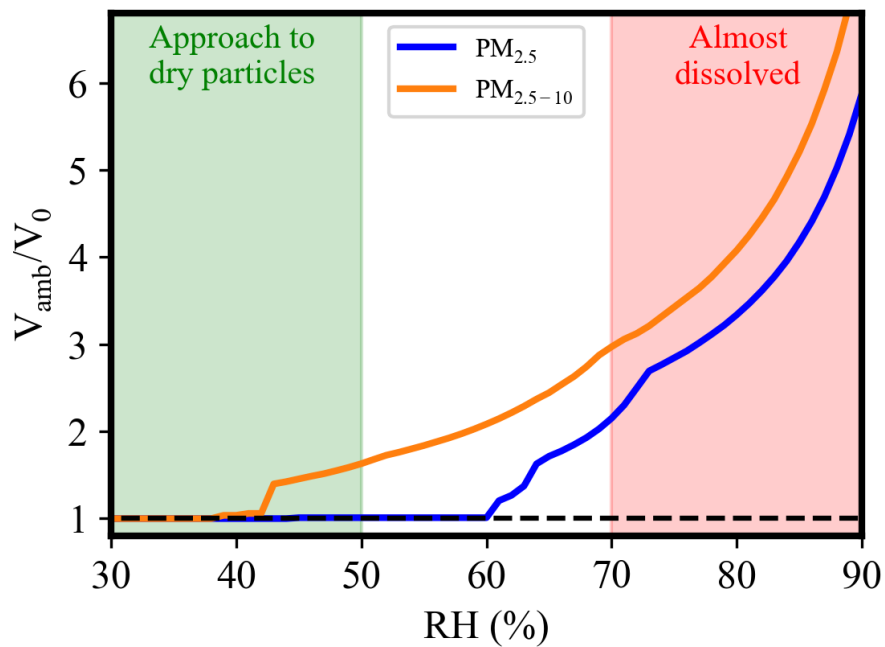
475   **Figure 5: The volume ratio of a given soluble composition as a function of RH under thermodynamic equilibrium calculated using E-AIM at 298.15 K. (composition is the averaged IC data with a molarity ratio of Na^+:NH_4^+:Cl^-:SO_4^{2-}:NO_3^- as 7:229:0:71:94 for $PM_{2.5}$, and 65:59:16:19:70 for $PM_{2.5-10}$.)**